PHYSICAL REVIEW B **84**, 085202 (2011)

Optically pumped InP: Nuclear polarization from NMR frequency shifts

K. L. Sauer,[1,2] C. A. Klug,[1] J. B. Miller,[1,*] and J. P. Yesinowski[1]

[1]*Naval Research Laboratory, Chemistry Division, Code 6122, Washington, DC 20375-5342, USA*

[2]*Department of Physics and Astronomy, George Mason University, 4400 University Drive MS 3F3, Fairfax, Virginia 22030, USA*

(Received 8 March 2011; revised manuscript received 14 July 2011; published 19 August 2011)

There are a number of mechanisms that can produce frequency shifts in the NMR spectra of optically pumped semiconductors, including the hyperfine interaction, nuclear dipolar fields, and indirect or J couplings. Using optically pumped Fe-doped InP, we explore how to experimentally distinguish these shift mechanisms from one another, and then exploit the shifts to measure the absolute nuclear polarization. Furthermore, we optically pump, using circularly polarized light, at a much lower field (2.35 T) than previous work, permitting us to explore the field dependence of the nuclear polarization rate, the spin-lattice relaxation time, and the NMR photon energy spectrum. We measure similar polarizations as obtained at higher fields, but with a significantly faster nuclear polarization rate, making operation at lower fields attractive for optically pumped InP as a source of nuclear spin polarization.

DOI: 10.1103/PhysRevB.84.085202 PACS number(s): 76.60.Jx, 33.80.Be, 78.30.Fs

I. INTRODUCTION

Since the first nuclear magnetic resonance (NMR) work on optical pumping in semiconductors,[1] much effort has gone into understanding the mechanisms behind the creation of nuclear polarization and measuring the magnitude of the nuclear polarization.[2] In part, these latter studies have been motivated by potential applications[3] of the high nuclear polarizations obtained through optical pumping to NMR signal enhancement,[4–6] spintronics,[7,8] quantum computing,[9–11] and other areas.

While much of the recent work in optical pumping of semiconductors has centered on studies of GaAs, InP has also garnered some interest. InP has some advantages for applications in NMR signal enhancement[4] because of the presence of a spin-1/2 isotope ^{31}P with 100% natural abundance. The lack of a quadrupole moment may be expected to make spin-1/2 nuclei less susceptible to distortions near the surface of semiconductor crystals that can inhibit spin diffusion among quadrupolar nuclei in this critical region of the material. For NMR signal enhancement applications, high nuclear polarization at the surface of the semiconductor crystal and rapid polarization transfer from the crystal to the material being studied are of utmost importance.

In most NMR studies, determination of the magnitude of nuclear polarization in optically pumped systems is based on measurement of the NMR signal amplitude and estimates of the optically pumped volume. In contrast, Paravastu and Reimer probed the nuclear polarization in GaAs using the asymmetry of the ^{71}Ga quadrupolar satellite transitions induced by the low spin temperatures from optical pumping.[12] They noted that the growth of polarization with optical pumping time as obtained from the satellite transition asymmetry was not in quantitative agreement with the growth of signal amplitude, calling into question estimates of polarization from signal amplitude alone.

A number of authors have remarked on the hyperfine contact shift observed in some semiconductors during light irradiation,[13–16] particularly as the shift is proportional to the electron's polarization. Coles used this shift to make an absolute measurement of electron polarization in GaAs.[16] He noted that a resonance shift that persisted at long pumping times might have its origins in the nuclear polarization,[17] but no quantitative work on the origins of these long-time shifts has appeared.

We show, using ^{31}P NMR of InP, that these long-time shifts can in fact be used to measure nuclear polarization. We theoretically predict the size of these shifts, which are due to long-range nuclear interactions in a polarized sample. Furthermore, we describe how to experimentally distinguish shifts from different possible sources, including polarized electrons and both nuclear species. We also distinguish between long-range and short-range nuclear interactions and describe the shifts due to each, and the information to be extracted from them. Using the long-time shifts, we explore how the ^{31}P polarization depends on pumping time and the photon energy, and compare this to how the net signal size depends on pumping time and photon energy.

II. PRINCIPLES

The absorption of circularly polarized light by a semiconductor excites electrons from the valence band to the conduction band and simultaneously transfers angular momentum from the photons to the electrons. In a III-V direct gap semiconductor, transitions between energy levels at the top of the valence band and the bottom of the conduction band can be well modeled by transitions between the $^2P_{3/2}$ and $^2S_{1/2}$ states in a spherically symmetric atom.[2,18,19] With near band-gap irradiation parallel to the applied magnetic field B, the expectation value of the electron's angular momentum $\mathbf{J}$ along the direction of the field is[20]

$$\langle J_z\rangle = \frac{\tau_s}{\tau+\tau_s}\langle J_z\rangle_i + \frac{\tau}{\tau+\tau_s}\langle J_z\rangle_{\rm eq}, \qquad (1)$$

where τ is the lifetime of the electron in the conduction band and τ_s is the electron's spin-relaxation time; typical values for these times at high field and low temperature are on the order of nanoseconds in InP.[21] The initial polarization just after optical excitation is $\langle J_z\rangle_i = \mp\frac{1}{4}$ for $\sigma_\pm^B$ helicity of light,[2] where σ_+^B corresponds to circularly polarized light with angular momentum parallel to the direction of the magnetic field

and σ_-^B corresponds to antiparallel angular momentum. Under typical experimental conditions, $\langle J_z\rangle_i$ is larger than the thermal equilibrium electron polarization $\langle J_z\rangle_{\rm eq} = -\frac{1}{2}\tanh(\frac{g^*\mu_B B}{2kT})$, where the effective g^* factor of the conduction electron multiplies the Bohr magneton μ_B and kT corresponds to thermal energy. For InP, the measured values of g^*[22–24] are consistent with the theoretical prediction[25] of $g^* = 1.20$.

Polarized electrons bind to trapping sites, corresponding to optically relevant defects (ORDs),[2,13] permitting prolonged interaction with surrounding nuclei. Local nuclear polarization results and the polarization then extends into the sample through spin diffusion.[26,27] The cross relaxation between the trapped s electrons and the nuclei is mediated through the magnetic dipole Hamiltonian, which can be broken down into two terms[28]:

(1) The Fermi contact, or isotropic, term[29]

$$\mathcal{H}_{\rm iso} = \frac{2\mu_0}{3} g_0\mu_B\gamma_S\hbar|\psi(r)|^2\mathbf{J}\cdot\mathbf{S}, \qquad (2)$$

where $\psi(r)$ is the wave function of the electron at the nucleus with spin $\mathbf{S}$, μ_0 is the permeability of free space, g_0 is the free-electron g factor, and γ_S is the nuclear gyromagnetic ratio;

(2) the anisotropic term, often simply called the "dipolar" term,

$$\mathcal{H}_{\rm an} = \frac{\mu_0}{4\pi} g_0\mu_B\gamma_S\hbar\left[3\frac{(\mathbf{J}\cdot\mathbf{r})(\mathbf{S}\cdot\mathbf{r})}{r^5} - \frac{\mathbf{J}\cdot\mathbf{S}}{r^3}\right], \qquad (3)$$

where $\mathbf{r}$ is the displacement vector between the electron and the nucleus.

Expressing $\mathbf{J}\cdot\mathbf{S} = J_zS_z + \frac{1}{2}(J_+S_- + J_-S_+)$, it is clear that the exchange of polarization through the isotropic term [Eq. (2)] would result in angular momentum $\langle S_z\rangle$ generated by the flip-flop terms having the same sign as $\langle J_z\rangle$. The more complicated anisotropic term [Eq. (3)] also contains these flip-flop terms $J_\pm S_\mp$, as well as single and simultaneous flip terms,[30] and so the predicted relative sign of the exchanged polarization relies on further assumptions. Under the assumption of random fluctuations with very short correlation times, the anisotropic term would lead to $\langle S_z\rangle$ of opposite sign as $\langle J_z\rangle$.[31,32]

As shown in Fig. 1, after σ_-^B pumping the ^{31}P nuclear signal in Fe-doped InP has the same sign as the thermal equilibrium signal, while for σ_+^B pumping the NMR signal is inverted. Previous researchers[33,34] have observed the same relative phases between optically pumped and thermal equilibrium signals in Fe-doped InP. Full thermal equilibrium is $\langle S_z\rangle_{\rm eq} = \frac{1}{2}\tanh(\frac{\gamma_P\hbar B}{2kT})$, where γ_P is the ^{31}P gyromagnetic ratio. Given the positive gyromagnetic ratio of ^{31}P, this implies that $\langle S_z\rangle$ is positive for σ_-^B pumping, and negative for σ_+^B pumping. Given Eq. (1), $\langle J_z\rangle$ is expected to be positive for σ_-^B pumping and negative for σ_+^B. This agreement in sign between $\langle S_z\rangle$ and $\langle J_z\rangle$ is consistent therefore with polarization generated through a Fermi-contact interaction [Eq. (2)].

A. Energy shifts with magnetic field

As the magnetic field is increased from zero, the valence and conduction bands are broken into highly degenerate subbands.[35] At high fields, the effects of the creation of these subbands on the NMR photon energy spectrum is twofold: the optical band gap changes, thus shifting the spectrum, and

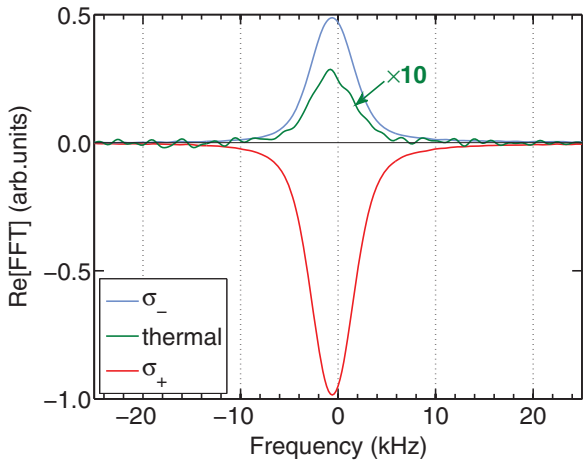

FIG. 1. (Color online) ^{31}P NMR spectra obtained after $\tau_L = 600$ s of σ_+^B (red, lower curve) or σ_-^B (blue, upper curve) helicity pumping at 1.408 eV are compared to the thermal equilibrium spectrum obtained after 3600 s in the dark (green, middle curve). The sequence as shown in Fig. 4(d), with $\tau_D = 1$ s and a single 17° excitation pulse, was used to create the spectra. Note that the σ_-^B spectrum has the same phase as the thermal equilibrium spectrum, which is consistent with $\langle J_z\rangle_i = +\frac{1}{4}$ and a Fermi-contact interaction.

there appears a complex semioscillatory structure with super-band-gap irradiation.[33,34,36,37] An example of such structure can be seen in the 9.39 T data[33] shown in Fig. 2. It has recently been shown that the structure seen in the NMR photon energy spectrum is well correlated to optical absorption measurements,[36] giving an overall picture consistent with the existence of these subbands.

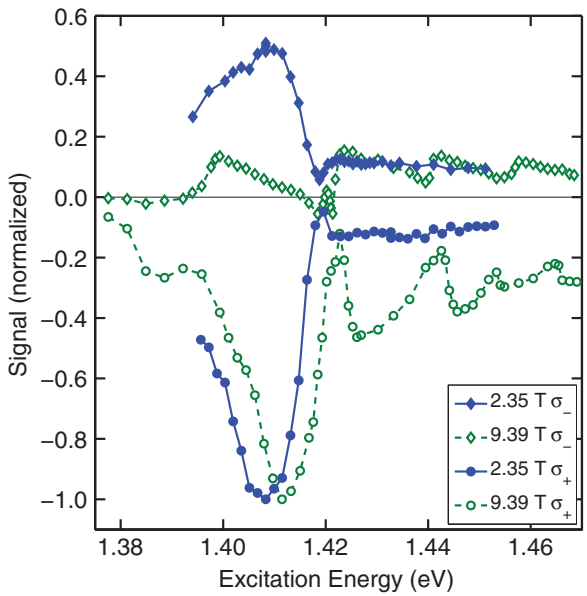

FIG. 2. (Color online) ^{31}P NMR signal amplitude as a function of photon energy and helicity of the optical pumping light. Notice, as the field is increased, the overall shift in the structure and the emergence of complex semioscillatory data for super-band-gap irradiation ($E_g = 1.424$ eV[38,39]). Data at 9.39 T are taken from Ref. 33. Data at 2.35 T are taken with the same material using the sequence shown in Fig. 4(b) with $\tau_L = 100$ s.

As the field decreases, the spacing between the subbands decreases. Using the measurements and theoretical predictions for InP of Ref. 38 for σ_+^B light, one would expect three interband transitions within 30 meV of the lowest energy transition at 9.39 T. For our experimental field of 2.35 T, the number of interband transitions within this interval doubles. There is, however, no structure observed for super-band-gap irradiation at 2.35 T, implying that the numerous subbands overlap at this field.

As the magnetic field is increased, the optical band gap also increases.[35,38] This effect is particularly noticeable in the σ_+^B NMR photon energy spectrum of Fig. 2. As the field is increased from 2.35 to 9.39 T, the gross features of the σ_+^B spectrum are shifted upward by ∼3 meV. The gross features are determined with respect to the band-gap energy. With photon energies just below the band-gap energy, optical pumping efficiency[33] is decreased but the penetration depth is increased, resulting in a large net NMR signal. In contrast, with photon energies above the band gap, the optical pumping efficiency is increased yet the penetration depth is decreased, resulting in a smaller NMR signal. The distinctive drop in signal in going to photon energies above the band gap served as our marker to judge the shift in the spectrum. Using the theoretical calculations of Ref. 38 for the lowest energy interband transition between 0 and 8 T, the increase in the transition energy with field is 0.21 meV/T, resulting in a predicted shift of 1.5 meV between the two spectra of Fig. 2, on the same order as what we observe.

B. NMR frequency shifts

The NMR Hamiltonian for phosphorus nuclei in InP can be written as

$$\mathcal{H}^S = \mathcal{H}_0^S + \mathcal{H}_{dd}^{SS} + \mathcal{H}_{dd}^{IS} + \mathcal{H}_J^{IS} + \mathbf{H}_h^{JS}, \tag{4}$$

where $\mathcal{H}_0^S$, the Zeeman interaction, combines both the applied static magnetic field and chemical shift interactions, $\mathcal{H}_{dd}^{SS}$ and $\mathcal{H}_{dd}^{IS}$ are the P-P and In-P dipolar couplings, respectively, $\mathcal{H}_J^{IS}$ is the In-P indirect or J coupling, and $\mathbf{H}_h^{JS}$ is the hyperfine coupling responsible for the hyperfine shift. The hyperfine coupling is given a different symbol to indicate it is observed only during light irradiation; all other interactions are always observed. In the high-temperature limit only $\mathcal{H}_0^S$ and $\mathbf{H}_h^{JS}$ can produce a frequency shift of the resonance, while all the interactions can broaden the NMR spectrum, with the In-P J coupling and dipolar coupling dominating the phosphorus NMR linewidth.[40–44] At low spin temperatures, these interactions also have the potential to shift the resonance in addition to affecting the linewidth. We will show that if the various interactions can be untangled, the resonance shift can be used as a measure of the local spin temperature.

1. *Hyperfine shift*

The nuclei close to a trapped polarized electron experience a magnetic field via the Fermi-contact Hamiltonian [Eq. (2)].[45] For σ_+^B pumping, the average magnetic moment of the optically excited electron should be in the same direction as the magnetic field, resulting in an increase in the local magnetic field or a positive frequency shift of the NMR signal. Especially for short pumping times, we observe a positive frequency shift of the ^{31}P NMR signal when the pumping light is left on during signal acquisition compared to when the pumping light is turned off just before signal acquisition. The frequency of the latter signal does not vary with an increase of up to 1 s in the delay, τ_D, defined in Fig. 4, between turning the light off and acquiring the signal. Therefore, given the short electron spin-relaxation time, we attribute this positive frequency shift to the hyperfine shift. Moreover, at longer pumping times the nuclear polarization spin-diffuses away from the regions near the trapped electrons to more distant regions. Thus, one would expect the observed frequency shift in the light to decrease with increased pumping time, an effect we observe, and which has also been seen in GaAs.[14,17]

The hyperfine shift is directly proportional to the electron's average polarization $\langle J_z\rangle$. As pointed out in Ref. 16, if there is no helicity dependence to the spin diffusion constant D, the electron's lifetime τ, or $\langle J_z\rangle_{\rm eq}$, the frequency shifts observed with the two different helicities, $\Delta\nu_{\sigma\pm}$, can be used to determine the electron's polarization. It is clear, however, for Fe-doped InP, the assumptions of helicity independence for the above quantities are not correct. If they were, the ratio of intensities of the ^{31}P NMR signals for the two helicities would be[16]

$$\left|\frac{S_{\sigma+}}{S_{\sigma-}}\right| = \left|\frac{\langle J_z\rangle_i(\sigma+) - \langle J_z\rangle_{\rm eq}}{\langle J_z\rangle_i(\sigma-) - \langle J_z\rangle_{\rm eq}}\right|, \tag{5}$$

$$\left|\frac{S_{\sigma+}}{S_{\sigma-}}\right| = \frac{1 - 2\tanh\left(\frac{g^*\mu_B B}{2kT}\right)}{1 + 2\tanh\left(\frac{g^*\mu_B B}{2kT}\right)}, \tag{6}$$

or in other words the magnitude of the positive helicity signal should be smaller than the magnitude of the negative helicity signal. We, along with Refs. 33 and 34, observe the opposite. This challenges the assumptions made about helicity independence of the parameters. Particularly, the assumption regarding τ is suspect, as a helicity dependence of the recombination rate has been observed in n-type InP.[46] Therefore we cannot measure the absolute electron polarization in Fe-doped InP using the hyperfine shift alone. Nevertheless, the hyperfine shift is proportional to the electron polarization, and in the limit that the electron's polarization is much higher than thermal equilibrium and the spin diffusion is helicity independent, the ratio of the hyperfine shifts $\frac{\Delta\nu_{\sigma+}}{\Delta\nu_{\sigma-}}$ would be equal to the ratio of nuclear signals $\frac{S_{\sigma+}}{S_{\sigma-}}$. We will present results in Sec. IV B addressing this point.

2. *Shifts from long-range nuclear interactions*

After optical pumping has been turned off, there remains a long-lived shift which may be attributed to the magnetic field created by the nuclear polarization. In the following we assume the electron has already depolarized, since the electron spin-relaxation time is so short. In general the shape of the pumped region, defined by the diameter of the optical pumping beam and the penetration depth, resembles a pancake-like structure since the penetration depth is at least two orders of magnitude smaller than the beam width. If the cross-relaxation rate is slow compared to the spin-diffusion rate, the pancake will be uniformly polarized at all pumping times. Otherwise, at short pumping times it will have local pockets of strong magnetization around the ORD's. As the pumping time

increases, these local pockets, which we model as uniformly distributed, expand out radially until they fill the optically pumped region. In both cases, of uniform polarization or of localized pockets, our macroscopic model for the frequency shifts applies.

The NMR frequency shift is observed after the phosphorus magnetic moment is tipped out of alignment with the static magnetic field $B_0\hat{z}$ associated with the Zeeman Hamiltonian $\mathcal{H}_0^S$. The net magnetic moment $\mathbf{M} = \gamma_P \hbar \sum_j \langle \mathbf{S}_j \rangle$ precesses around $\hat{z}$ at an angular frequency of

$$\omega = \frac{d\phi}{dt} = \frac{d\mathbf{M}}{dt} \cdot \frac{\hat{z} \times \mathbf{M}}{M_\perp^2}, \tag{7}$$

where $\phi = \arctan \frac{M_y}{M_x}$ is the angle in the x-y plane of the transverse magnetic moment $\mathbf{M}_\perp \equiv \mathbf{M} - M_z\hat{z}$. We can also express this equation in the frame rotating with the Larmor angular frequency $\Omega = -\gamma_P B_0$,

$$\omega = \Omega + \frac{d\tilde{\mathbf{M}}}{dt} \cdot \frac{\hat{z} \times \tilde{\mathbf{M}}}{M_\perp^2}, \tag{8}$$

where $\tilde{\mathbf{M}} = \gamma_P \hbar \sum_j \langle \tilde{\mathbf{S}}_j \rangle$ and $\tilde{\mathbf{S}} = e^{-i\mathcal{H}_0^S t/\hbar} \mathbf{S} e^{i\mathcal{H}_0^S t/\hbar}$. Therefore from the evolution in time of the expectation value of $\tilde{\mathbf{M}}$ the NMR frequency shift can be calculated.

Following Ref. 32, the evolution in time of $\tilde{\mathbf{M}}$ due to nuclear dipolar coupling $\mathcal{H}_{dd}^{SS} + \mathcal{H}_{dd}^{IS}$ can be calculated through the Ehrenfest theorem

$$-i\hbar \frac{d\tilde{\mathbf{S}}_j}{dt} = \left[e^{-i\mathcal{H}_0^S t/\hbar} \left(\mathcal{H}_{dd}^{SS} + \mathcal{H}_{dd}^{IS} \right) e^{i\mathcal{H}_0^S t/\hbar}, \tilde{\mathbf{S}}_j \right]. \tag{9}$$

Because the dipolar Hamiltonian serves as a perturbation to $\mathcal{H}_0^S$, we can invoke the secular approximation, which is equivalent to retaining that part of the dipolar Hamiltonian which commutes with $\mathcal{H}_0^S$. We define this as the "truncated" dipolar Hamiltonian

$$\begin{aligned} \mathcal{H}_{dd}^{SS'} + \mathcal{H}_{dd}^{IS'} = -\frac{1}{2} \sum_j \gamma_P \hbar \mathbf{S}_j \cdot \Bigg\{ & \sum_{k \neq j} \frac{\mu_0 \gamma_P \hbar}{4\pi} \\ & \times \frac{\left(\frac{3}{2} S_{z,k} \hat{z} - \frac{1}{2} \mathbf{S}_k \right) [3(\hat{z} \cdot \hat{\boldsymbol{\mathcal{R}}}_{jk})^2 - 1]}{\mathcal{R}_{jk}^3} \\ & + \sum_i \frac{\mu_0 \gamma_I \hbar}{4\pi} \frac{I_{z,i} \hat{z} [3(\hat{z} \cdot \hat{\boldsymbol{\mathcal{R}}}_{ji})^2 - 1]}{\mathcal{R}_{ji}^3} \Bigg\}, \end{aligned} \tag{10}$$

where γ_I is the indium gyromagnetic ratio and $\boldsymbol{\mathcal{R}}_{ji} = \mathbf{r}_j - \mathbf{r}_i$ is the displacement vector between the jth phosphorus nucleus and the ith indium nucleus. Note that the expressions in curly braces can be thought of as a demagnetizing field[47] $\mathbf{B}_d(\mathbf{r}_j)$ acting on spin $\mathbf{S}_j$.

Using Eq. (9) and the truncated dipolar Hamiltonian given in Eq. (10), the equation of motion for a single spin in the rotating frame becomes

$$\frac{d\mathbf{S}_j}{dt} = \gamma_P \mathbf{S}_j \times \mathbf{B}_d(\mathbf{r}_j), \tag{11}$$

where for simplicity of notation the tildes are dropped from here onward. A similar equation can be written for the evolution of an indium spin $\mathbf{I}_i$ in the demagnetizing field. We therefore have a set of coupled equations corresponding to the number of spins in the solid sample. Due to the number of nuclei in a solid sample, Eq. (11) does not afford an exact solution; only spin systems with up to 14 spins have been calculated exactly.[48]

Therefore, in order to estimate the net shift due to polarized nuclei, we make several simplifying assumptions. For instance, if the expectation values of the individual indium spins are aligned with the field, $\langle \mathbf{I}_i \rangle = \langle I_{z,i} \rangle \hat{z}$, these expectation values do not change in time in the presence of other polarized indium or phosphorus nuclei. In this case evolution of the phosphorus spins due to the local magnetic field generated by the indium polarization is easily calculated, since the phosphorus spin equations are not coupled. As expressed in Eq. (10) the indium demagnetizing field is given as

$$\mathbf{B}_{d,I}(\mathbf{r}_j) = \hat{z} \sum_i \frac{\mu_0 \gamma_I \hbar}{4\pi} \frac{I_{z,i} [3(\hat{z} \cdot \hat{\boldsymbol{\mathcal{R}}}_{ji})^2 - 1]}{\mathcal{R}_{ji}^3}. \tag{12}$$

Note that the field expressed in the summation is equivalent to the z component of the magnetic field arising from a set of magnetic moments of value $\gamma_I \hbar I_{z,i} \hat{z}$ centered on the indium nuclei.

Furthermore, given the InP crystal symmetry and assuming the pocket grows radially, as we do, the demagnetizing field from the pocket will not contribute to a net shift. More formally, we break both the sums in $\mathbf{B}_d$ of Eq. (10) into two pieces, a sphere of radius r_0, half the distance between ORD's, centered on the jth phosphorus nucleus and the rest of the pumped region:

$$\sum_i = \sum_{i, \mathcal{R}_{ji} \leqslant r_0} + \sum_{i, \mathcal{R}_{ji} > r_0}, \tag{13}$$

$$\sum_{k \neq j} = \sum_{k, \mathcal{R}_{jk} \leqslant r_0} + \sum_{k, \mathcal{R}_{jk} > r_0}. \tag{14}$$

Because of the cubic symmetry of the InP zincblende lattice structure and spherical symmetry of the pocket, the first sum on the right-hand side in Eqs. (13) and (14) on average is zero. Therefore nearby nuclei do not contribute to the net nuclear magnetic field, although they may contribute to the dipolar broadening of the resonance. As discussed in more detail later, the field from the second sum we can approximate as coming from a magnetization distribution which is smooth, with a spherical hole in it of radius r_0 centered on the jth phosphorus nucleus.

The demagnetizing field from the phosphorus nuclei can also be greatly simplified if we assume the expectation value of the individual phosphorus nuclei point in the same direction, such that $\mathbf{S}_j \times \mathbf{S}_k = 0$. In this limit, the phosphorus magnetization in the $\hat{z}$ direction remains unchanged, and the equations of motion governing the individual phosphorus nuclei are decoupled, with an individual phosphorus nuclei $\mathbf{S}_j$ experiencing a phosphorus-induced demagnetizing field of

$$\mathbf{B}_{d,P}(\mathbf{r}_j) = \hat{z} \sum_{k \neq j} \frac{\mu_0 \gamma_P \hbar}{4\pi} \frac{\frac{3}{2} S_{z,k} [3(\hat{z} \cdot \hat{\boldsymbol{\mathcal{R}}}_{jk})^2 - 1]}{\mathcal{R}_{jk}^3}. \tag{15}$$

Note that the field expressed in the summation is equivalent to the z component of the magnetic field arising from a set of magnetic moments of value $\gamma_P \hbar \frac{3}{2} S_{z,k} \hat{z}$ centered on the phosphorus nuclei.

Equation (15) implies that the frequency shift would best be observed for small flip angles, so that a reasonable $S_{z,k}$ remains after radio-frequency excitation. The approximation of taking the individual spins to be pointing in the same direction is valid immediately after the sample is uniformly excited by an excitation pulse. (We take the dipolar effects during the excitation pulse to be negligible since the radio-frequency field strength is much larger than the demagnetizing field.) The signal quickly decays, due to dipolar broadening by In and P nuclei, on a time scale of $\tau_{\text{decay}} \sim 100\ \mu$s. Therefore, if the flip angle is small, and given the long-range nature of the demagnetizing field, it is reasonable to assume that individual spins remain parallel during this time. This is equivalent to assuming that $\gamma_P \Delta \mathbf{B}_d \tau_{\text{decay}} \ll 1$, where $\Delta \mathbf{B}_d$ represents the variation of the demagnetizing field over the irradiated region. Furthermore, with the use of a small flip angle, we avoid the instabilities predicted theoretically,[49] and observed experimentally,[50] with large flip angles applied to highly polarized spin systems.

With the above simplifications, particularly the phosphorus magnetic moments pointing in the same direction and the indium magnetic moments pointing in the z direction, the net frequency shift, from Eqs. (8) and (11), is

$$\omega = \Omega - \frac{\gamma_P}{M_\perp} \sum \gamma_P \hbar |\langle \mathbf{S}_j \rangle_\perp| B_d(\mathbf{r}_j), \tag{16}$$

where $\langle \mathbf{S}_j \rangle_\perp \equiv \langle \mathbf{S}_j \rangle - \langle \mathbf{S}_j \rangle \cdot \hat{z}$. With the nonlocal nature of B_d, the sum can be replaced by an integral so that

$$\omega = \Omega - \frac{\gamma_P}{M_\perp} \int |\boldsymbol{\mathcal{M}}_{P\perp}(\mathbf{r})| B_d(\mathbf{r}) d^3\mathbf{r}, \tag{17}$$

with phosphorus magnetization $\boldsymbol{\mathcal{M}}_P$ equal to the phosphorus magnetic dipole moment per unit volume. From Eq. (17), one can see how the frequency shift can serve as a metric of the demagnetizing field. In particular, it is proportional to the average of the demagnetizing field weighted by the local transverse phosphorus magnetization as compared to the net transverse magnetic moment, where we recognize that the net phosphorus magnetic moment $\mathbf{M} = \int \boldsymbol{\mathcal{M}}_P d^3\mathbf{r} = \gamma_P \hbar \sum_j \langle \mathbf{S}_j \rangle$.

In the next section we find the demagnetizing field, and therefore the shift, due to the polarized indium nuclei and in the following section the shift due to polarized phosphorus nuclei.

a. NMR shifts from polarized indium nuclei.. As discussed above, we can approximate the demagnetizing field from polarized indium nuclei as coming from a magnetization distribution which is smooth, $\boldsymbol{\mathcal{M}}_I = \mathcal{M}_I \hat{z}$, with a spherical hole in it of radius r_0 centered on the jth phosphorus nucleus. The indium magnetization is given by

$$\mathcal{M}_I = \gamma_I \hbar \langle I_z \rangle \frac{4}{a^3}, \tag{18}$$

since the combined density of each species of indium magnetic moments is 4 per unit cell, where the volume of the unit cell is a^3.

The field from this magnetized distribution can be calculated using[51]: (i) a bound current density integrated over the entire volume $\mathbf{J}_b = \nabla \times \boldsymbol{\mathcal{M}}_I = \hat{x} \frac{\partial \mathcal{M}_I}{\partial y} - \hat{y} \frac{\partial \mathcal{M}_I}{\partial x}$; and (ii) two bound surface currents, one integrated over the exterior surface and one integrated over the surface of the spherical hole $\mathbf{K}_b = \boldsymbol{\mathcal{M}}_I \times \hat{n}$. Here $\hat{n}$ is the unit vector normal to the surface. The bound surface current at the surface of the hollow sphere is equivalent to that from a sphere magnetized in the opposite direction and therefore contributes a field $\mathbf{B}_{\text{hollow}} = -\frac{2}{3}\mu_0 \boldsymbol{\mathcal{M}}_I(\mathbf{r}_j)$. We have approximated the sphere of opposite magnetization as uniform, a reasonable approximation if the distance separating the ORDs is much smaller than the penetration depth. The field from the bound current density outside the hole and the bound surface current at the edges of the polarized region we will combine and label as $\mathbf{B}_{\text{out}}$, so that

$$B_{d,I}(\mathbf{r}_j) = -\tfrac{2}{3}\mu_0 \overline{\mathcal{M}}_I(\mathbf{r}_j) + \mathbf{B}_{\text{out}}(\mathbf{r}_j) \cdot \hat{z}, \tag{19}$$

where $\mathcal{M}_I(\mathbf{r}_j)$ is averaged over a sphere of radius r_0 and centered at the jth phosphorus nucleus.

The field $\mathbf{B}_{\text{out}}(\mathbf{r}_j)$ is

$$\mathbf{B}_{\text{out}}(\mathbf{r}_j) = \frac{\mu_0}{4\pi} \int_{\text{sample}} \frac{\mathbf{J}_b \times \hat{\mathcal{R}}}{\mathcal{R}^2} d^3r' + \frac{\mu_0}{4\pi} \int_{\text{edges}} \frac{\mathbf{K}_b \times \hat{\mathcal{R}}}{\mathcal{R}^2} d^2r', \tag{20}$$

where $\mathcal{R} \equiv \mathbf{r}_j - \mathbf{r}'$. Because the magnetization is only in the $\hat{z}$ direction the second integral is only over the edges of the wafer sample, not the flat surfaces. Taking only the z direction we find

$$\mathbf{B}_{\text{out}}(\mathbf{r}_j) \cdot \hat{z} = \frac{\mu_0}{4\pi} \int_{\text{sample}} \frac{\hat{\mathcal{R}} \cdot \left(\hat{y} \frac{\partial \mathcal{M}_I}{\partial y} + \hat{x} \frac{\partial \mathcal{M}_I}{\partial x} \right)}{\mathcal{R}^2} d^3r' - \frac{\mu_0}{4\pi} \int_{\text{edges}} \frac{\mathcal{M}_I (\hat{\mathcal{R}} \cdot \hat{n})}{\mathcal{R}^2} d^2r'. \tag{21}$$

The variation of $\mathcal{M}_I$ in the x-y plane is determined by the shape of the laser beam, which in our case is Gaussian in intensity, corresponding to the TEM_{00} mode of the laser. Before irradiating the sample, the laser beam is expanded to a width of $w = 3.7$ mm, which is much larger than the penetration depth of the beam into the sample, and therefore one would expect both integrals to have a negligible contribution to B_I compared to the sphere of opposite magnetization. In order to get a sense of the neglected contribution from $\mathbf{B}_{\text{out}}$, we simplified the optically pumped region to be a cylinder of uniform magnetization of diameter 3.7 mm and ranging in depth from 2 to 40 μm,[33] and calculated the field $\mathbf{B}_I(\mathbf{r}_j) \cdot \hat{z}$ with and without the contribution from $\mathbf{B}_{\text{out}}$. Using the sphere alone, in this scenario, overestimates the average calculated field by only 4% at the highest penetration depth; the overestimation decreases with decreasing penetration depth.

Therefore for short penetration depths, the demagnetizing field given in Eq. (19) reduces to

$$B_{d,I}(\mathbf{r}_j) = -\tfrac{2}{3}\mu_0 \overline{\mathcal{M}}_I(\mathbf{r}_j). \tag{22}$$

For uniform indium and phosphorus polarization, and using Eqs. (17), (22), and (18), the shift in the absolute NMR frequency is

$$\Delta\nu_{\rm In} = -\mu_0\gamma_I\gamma_P\hbar\frac{4}{3\pi a^3}\langle I_z\rangle = -8.02\ {\rm kHz}\frac{\langle I_z\rangle}{I}. \quad (23)$$

We define the fractional indium polarization as $\frac{\langle I_z\rangle}{I}$. Assuming transfer of angular momentum, or spin, mediated through the Fermi contact interaction, Eqs. (23) and (18) predict that for σ_+^B light ($\frac{\langle I_z\rangle}{I}$ negative) the net field should increase, or the NMR frequency should increase, and that for σ_-^B the NMR frequency should decrease. In order to separate out the shift due to indium nuclei versus the shift due to phosphorus nuclei, we saturate the indium nuclei just before acquiring a ^{31}P signal and compare it to the same experiment with saturation of indium nuclei before optical pumping begins.

b. NMR shifts from polarized phosphorus.. In a similar manner, but using Eq. (15), the demagnetizing field due to polarized phosphorus can be calculated to be

$$B_{d,P}(\mathbf{r}_j) = -\frac{2}{3}\mu_0\gamma_P\hbar\left(\frac{3}{2}\overline{\langle S_z\rangle}\frac{4}{a^3}\right). \quad (24)$$

The expectation value of $\langle S_z\rangle$ is averaged over a sphere of radius r_0 centered at the jth phosphorus nucleus. For uniform phosphorus polarization, and using Eqs. (17) and (24), the shift in the absolute NMR frequency is

$$\Delta\nu_P = -\mu_0\gamma_P^2\hbar\frac{2}{\pi a^3}\langle S_z\rangle = -2.46\ {\rm kHz}\frac{\langle S_z\rangle}{S}. \quad (25)$$

The fraction $\frac{\langle S_z\rangle}{S}$ represents the fractional phosphorus polarization *after* the applied pulse. As with the shift due to indium polarization for σ_+^B light, the net field should increase, or the NMR frequency should increase, and that for σ_-^B the NMR frequency should decrease.

3. Shifts from short-range nuclear interactions

Because of the symmetry of the crystal, the dipolar coupling only creates a significant frequency shift in the NMR signal for long pumping times and through long-range interactions. There are, however, frequency shifts in addition to the hyperfine shift that appear only for short pumping times. We associate these shifts with a short-range interaction, such as the J coupling between the indium and phosphorus nuclei described below.

High nuclear polarizations can directly affect the shape of NMR spectra in multilevel systems. For example, asymmetry in the satellite transition intensities has been observed in strained GaAs at low spin temperatures created by optical pumping.[12] In the present case, the two levels of our spin-1/2 system (^{31}P) can be split into sublevels by interaction with other nuclei. In addition to the nuclear dipole-dipole interaction discussed in the previous section, the indirect spin-spin coupling, or J coupling, will also influence the shape of the ^{31}P NMR spectrum in InP. Previous work indicates the In-P dipolar couplings and J couplings are of similar magnitude and partially cancel.[40]

The J coupling is a bilinear interaction where the interaction of the nuclear spins is mediated by the valence electrons. Like the hyperfine interaction it can be separated into two components: the isotropic component, analogous to the contact hyperfine interaction, and the anisotropic component, analogous to the dipolar hyperfine interaction. As with the hyperfine interaction, the isotropic component of the J coupling has no spatial orientation dependence, whereas the anisotropic component has the same orientation dependence as the dipolar interaction. Directly bonded atoms usually dominate the J coupling; therefore we consider only the four indium atoms directly bonded to phosphorus here. Because of the symmetry of the zincblende lattice and the orientation of our InP crystal, the nearest indium neighbors do not contribute to the anisotropic J coupling (or dipolar coupling); therefore we will not consider this interaction further.

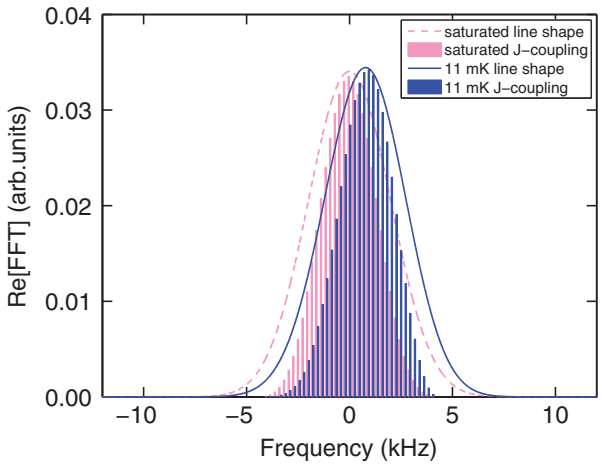

FIG. 3. (Color online) Calculated ^{31}P NMR line shape due to ^{115}In-^{31}P J coupling illustrating the resonance shift of 730 Hz on cooling the indium spins from the saturated state to 11 mK. The vertical bars show the intensities of the $4(2I)+1$ J-coupling peaks; the overall line shape is obtained by broadening the individual peaks to give an envelope that matches the observed linewidth of 4.65 kHz.

The In-P isotropic J coupling $\mathcal{H}_{J^{\rm iso}}^{IS} = J^{\rm iso}\mathbf{I}\cdot\mathbf{S}$ splits the energy levels of the phosphorus resonance, resulting in a band of peaks symmetrically distributed about the unsplit resonance position. With four magnetically equivalent indium nearest neighbors, assuming all to be ^{115}In (96% natural abundance), the phosphorus resonance is split into $4(2I)+1$ peaks separated by $|J^{\rm iso}| = 224\pm5$ Hz.[44] (In static experiments, other broadening mechanisms do not allow the resolution of these peaks.) In the high-temperature limit, created by saturating the ^{115}In spins, the $2I+1$ energy levels are all equally populated, resulting in an approximately Gaussian distribution of peak intensities symmetric about the unsplit resonance position. At low spin temperature the energy levels are no longer equally populated and the distribution of peak intensities is no longer symmetric about the unsplit resonance position. In the zincblende lattice the indium nuclear quadrupole coupling constant is zero and the energy levels are equally spaced. Then an optically pumped spin temperature of 11 mK results in an indium polarization of $\frac{\langle I_z\rangle}{I} = 5\%$ between any two adjacent energy levels and redistributes peak intensities such that the center-of-mass of the phosphorus resonance is shifted by 730 Hz, as shown in Fig. 3. The direction of the shift cannot be predicted because the sign of $J^{\rm iso}$ is not known; however, measurement of the shift will reveal the sign of $J^{\rm iso}$. The

redistribution of peak intensities will also change the resonance shape. At 11 mK the resonance is narrowed by 50 Hz, a very small narrowing compared to the additional broadening from other mechanisms.

III. EXPERIMENT

Optical pumping experiments were performed at photon energies of either 1.408 eV, representative of sub-band-gap irradiation, or 1.428 eV, representative of super-band-gap irradiation, except where noted. Our primary interest is in super-band-gap irradiation, where previous research has demonstrated high nuclear polarization near the surface.[33] Because of their typically higher SNR, we display results from sub-band-gap irradiation, where the only observed effect of irradiation energy is on the signal amplitude.

The goal of our experiments is to find how the frequency of the signal from the irradiated part of the sample separately depends on the electron and nuclear polarizations. Therefore we are interested in the frequency of the signal with high polarization with respect to the frequency of the signal with the relevant polarization approaching zero; this shift is calculated in the Principles section. Experimentally we focus on taking the difference in measured frequencies between two contrasting experiments. For the hyperfine shift we take the difference in frequency between when the light is left on during the acquisition (high electron polarization) versus when the light is off during the acquisition (electron polarization zero). For the indium shift we take the difference in frequency between when indium is saturated before pumping (high indium polarization) and when indium is saturated after pumping, but before acquisition (indium polarization zero). For the phosphorus shift, since this is our signal medium, we have no equivalent zero phosphorus polarization signal to serve as a reference. One might use the thermal equilibrium signal as an approximation for the zero phosphorus polarization signal, but it is difficult to obtain the thermal equilibrium signal only from the region which is normally illuminated, without moving to the complexities of an imaging experiment.[33] Therefore we compare the phosphorus frequency measured for σ_+^B light with that for σ_-^B light, with the indium saturated just before data acquisition in the dark.

All experiments were performed at 2.35 T (40.5 MHz for ^{31}P) using a Tecmag console. The sample was maintained at 5–10 K in either a Helitrans vacuum cryostat or a Janis gas flow cryostat containing a home-built double resonance NMR probe. A Spectra Physics model 3900S Ti:sapphire laser with typical intensity at the sample of 3.4 W/cm^2 was used for all experiments.

The semiconductor used in this work was a fragment of 348 μm thick (100) orientation Fe-doped semi-insulating InP (Showa Denko lot 60706).[33] The sample was prepared for study by thoroughly rinsing with petroleum ether, acetone, and methanol to remove dirt and other surface contaminants followed by etching in a 1 wt% Br_2/methanol solution for 30 min, followed by additional rinsing. The sample was then mounted with Apiezon N grease onto a sapphire block which was thermally anchored in the NMR probe.

We applied either single or double radio-frequency pulses to resonantly excite a phosphorus NMR signal. The double radio-frequency pulses were used to create an echo signal as shown in Figs. 4(a)–4(c), and were chosen to have a ∼90° excitation for the first pulse, ∼180° excitation for the second pulse, with a wait time between them of 150 μs. Pulse durations were typically 5 μs for the first pulse and 10 μs for the refocusing pulse. Values for n and m in Fig. 4, the number of saturation pulses, were in the range of 10–100. These echo sequences, in combination with phase cycling that isolated the echo and reduced probe ringing, were used for studies that included very short optical pumping times, where the NMR signal is small and the residual probe ringing prohibitively long. For long optical pumping times (>200 s), where the NMR signal is large, a single echo or train of FID's was acquired.

For experiments focused exclusively on long pumping times, single pulse excitation of a single FID gave a signal with a sufficient signal-to-noise ratio to mask the effects of probe

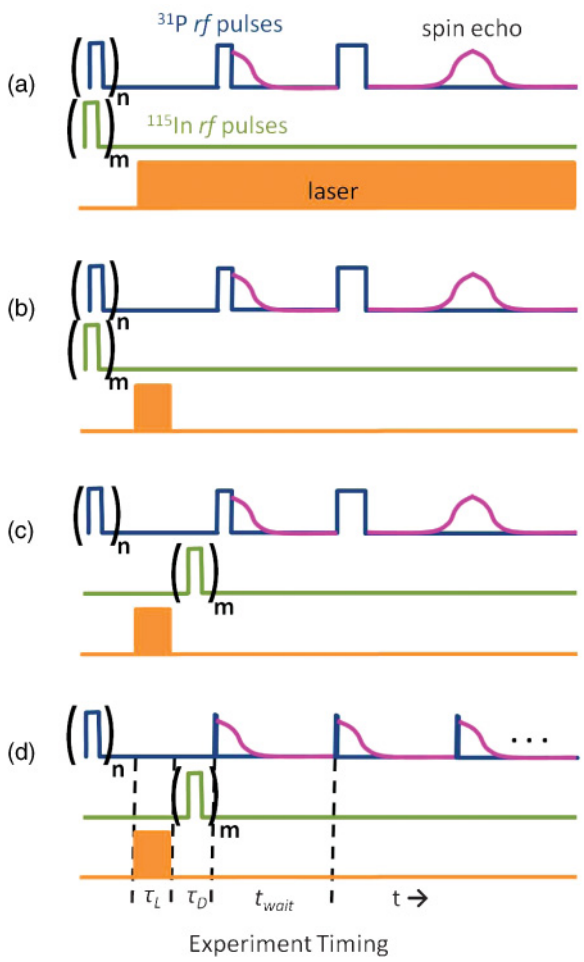

FIG. 4. (Color online) Pulse sequences used to obtain data. (a) Spin echo acquisition with ^{31}P and ^{115}In saturation prior to light irradiation, and light irradiation during signal acquisition. (b) Spin echo acquisition with ^{31}P and ^{115}In saturation prior to light irradiation, and signal acquisition in the dark. (c) Spin echo acquisition with ^{31}P saturation prior to light irradiation and ^{115}In saturation subsequent to light irradiation but prior to signal acquisition in the dark. (d) Small flip angle pulse FID acquisition with ^{31}P saturation prior to light irradiation and ^{115}In saturation subsequent to light irradiation but prior to signal acquisition in the dark.

ringing. Furthermore, to study the frequency shift induced by phosphorus magnetization remaining along the static magnetic field, a single short radio-frequency pulse, corresponding to a rotation less than 20°, was applied to generate the NMR signal. As shown in Fig. 4(d), a series of short pulses, with observation of the NMR signal between them, allowed us to monitor this frequency shift as the aligned magnetization is destroyed.

Phasing of the ^{31}P NMR spectra was accomplished with identical zero-order phase correction parameters for Fig. 1 and for the data for a given circular polarization in experiments incrementing some variable (Figs. 5, 7, and 8). In some cases, the relative phase of the ^{31}P NMR signals resulting from σ_+^B and σ_-^B helicity light showed small differences, up to 30°, from the 180° phase difference seen in Fig. 1. However, careful measurements focused on accurately determining the relative phase as a function of pumping time, light helicity, and photon energy found differences less than 10°. Therefore, we attribute larger observed phase changes to experimental artifacts such as changes in probe tuning and spectrometer reference phase instabilities.

We define the strength of the quadrature-detected NMR signal as the peak amplitude of the Fourier transform of the complex time domain data. The various shift mechanisms described in the Principles section result in shifts on the order of the size of the linewidth or less. To measure such relatively small shifts, we fit the complex time domain data, obtained through quadrature detection, to a complex sinusoid multiplied by the appropriate envelope function, depending on whether the signal resulted from a single pulse or double pulses. Using double pulses, corresponding to the creation of an echo after the second pulse, we find that the ^{31}P T_2 and T_2^* are comparable. The echo is modeled as a Gaussian centered at the time of echo formation and which is multiplied by an exponentially decaying function. The Gaussian is characterized by the time constant T_2^* with an average value of 190 μs, and the exponential decay by T_2 with an average value of 250 μs. For data sets corresponding to a series of short pulses, we globally fit all the time domain data to a common decay shape, a common starting phase, and a common excitation pulse. Executing this global fit reduced the scatter in the frequency shift fit parameters.

IV. RESULTS AND DISCUSSION

A. Nuclear build-up and relaxation rates

The NMR signal builds up as a function of pumping time with a characteristic time constant T_b, and decays after pumping termination with the spin-lattice relaxation time constant T_1. We measure the build-up time constant using 1.428 eV pumping light. A potential complication is the contribution to the net NMR signal from the nonirradiated part of the sample as it returns to thermal equilibrium. To subtract out effects from this contribution we subtract data taken after σ_+^B pumping from data taken after σ_-^B pumping. Data are taken with the sequence shown in Fig. 4(d), with $\tau_D = 1$ s. In this case, the amplitude of the free induction decay is used as a measure of the signal intensity, so as to avoid the effects of the frequency shifts arising from opposite polarity nuclear

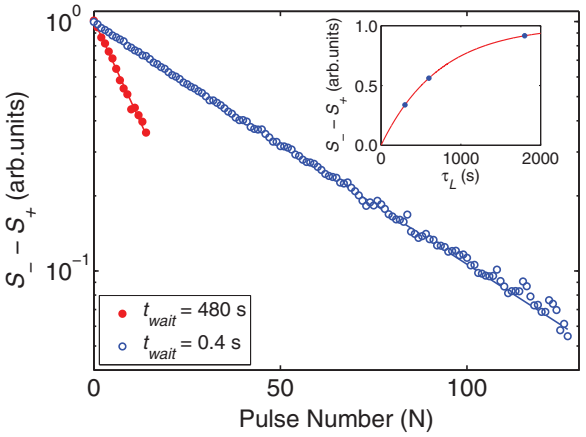

FIG. 5. (Color online) Measurement of the phosphorus T_1 at a temperature of 5 K, using sequence 4(d), corresponding to a succession of short rf pulses applied after $\tau_L = 600$ s of optical pumping at 1.408 eV and $\tau_D = 1$ s. Measurements were made for both helicities of light and the signals subsequently subtracted from one another to eliminate the contribution from thermal equilibrium signals. In the inset, measurement of the build-up time is shown.

polarization. As shown in the inset of Fig. 5, the subtracted amplitudes are fit to the function

$$S(\tau_L) = S_\infty(1 - e^{-\tau_L/T_b}), \tag{26}$$

with a time constant $T_b = 728 \pm 14$ s. Other researchers[33,34] working on optically pumped Fe-doped InP have also found their data fit well to Eq. (26), after accounting for the equilibrium signal from the nonirradiated part of the sample. At our lower operating magnetic field, the contribution of the equilibrium signal is less substantial and we find that the build-up time constants for data of each helicity taken separately are within 12% of the above stated value.

The T_1 was measured by comparing the decay of an optically pumped signal under a rapid succession of short rf pulses to the decay of the signal with long wait times $t_{\rm wait}$ between pulses [Fig. 4(d)]. In order to eliminate the thermal equilibrium contribution to the signal, we subtract data obtained after σ_+^B pumping from data obtained after σ_-^B pumping (see Fig. 5). Under this simplifying condition, and with the assumption that $t_{\rm wait}$ is much smaller than T_1, the difference in the signals ΔS decays as

$$\Delta S = S_0 x^N; \qquad x = \left(1 - \frac{t_{\rm wait}}{T_1}\right)\cos\theta, \tag{27}$$

where S_0 is the initial signal difference, θ is the pulse flip angle, and N is the pulse number starting from zero. As shown in Fig. 5, we simultaneously fit the two sets of subtracted data to Eq. (27), and calculate a T_1 of 8760 $\pm$ 120 s and a pulse angle of 12°.

Interestingly, both the build-up and T_1 times are much shorter, both by a factor of about 5, than those measured with the same material at a field of 9.39 T.[33] In particular, the shorter build-up time could be particularly advantageous for using InP as a polarizer. The shorter build-up time at 2.35 T is consistent with the faster cross relaxation predicted by an

electron-nuclear correlation time of $\sim 10^{-11}$ s, as has been previously found in these types of semiconductor systems.[27]

B. Hyperfine and indium-induced shifts

The frequency of the ^{31}P NMR signal resulting from short pumping times is shifted in the presence of light left on during data acquisition with respect to data acquired in the dark. This frequency shift corresponds to the hyperfine shift and is shown in Fig. 6 as the second set of bars. The optical pumping time is 5 s for these data, and the shifts are shown for different helicities and for different photon energies. In contrast to optically pumped GaAs,[52] our frequency shifts are quite comparable whether pumping above the band gap (1.428 eV) or below the band gap (1.408 eV); this implies that the polarization of the trapped electron multiplied by the fractional occupancy of the trapping site[29,53] is similar for the two photon energies.

While the NMR frequency changed in the presence of light during acquisition, the signal amplitude did not. Signal amplitudes obtained at two photon energies for both helicities, normalized by the signal size for σ_+^B light, are shown as the first set of bars in Fig. 6. For 1.428 eV pumping the ratio of the signal amplitudes with helicity, compared to the ratio of frequency

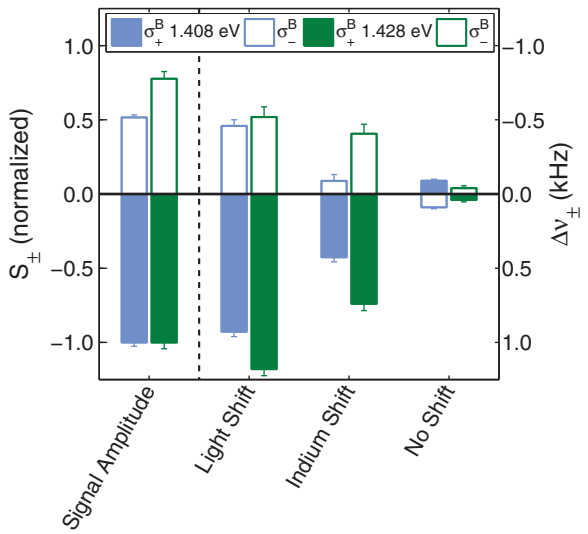

FIG. 6. (Color online) ^{31}P NMR signal parameters for 5 s of optical pumping and several different experimental conditions. "Signal Amplitude" is the magnitude of the ^{31}P NMR signal recorded during light irradiation with ^{31}P and ^{115}In saturation prior to pumping. "Light Shift" is the difference between the resonance frequencies recorded *during* light irradiation and recorded 0.1 s *after* light irradiation, with ^{31}P and ^{115}In saturation prior to pumping for both experiments. "Indium Shift" is the difference between the resonance frequencies with ^{115}In saturation *prior* to pumping and ^{115}In saturation *after* pumping, with both data sets recorded 0.1 s after light irradiation and ^{31}P saturation prior to pumping. "No Shift" is the resonance frequency recorded 0.1 s after light irradiation with ^{31}P saturation prior to and ^{115}In saturation after pumping, with "zero" frequency defined as the average of the resonance frequencies from the two light helicities. Data for optical pumping at 1.408 eV are in blue (left pair of bars in each group) and 1.428 eV are in green (right pair of bars in each group); σ_+^B pumping are the filled bars and σ_-^B the open bars.

shifts, is close to the value expected under high $\langle J_z \rangle_i$ and helicity independent diffusion, and for the high $\langle J_z \rangle_{\rm eq}$ at our experimental temperatures [Eq. (5), Sec. II B 1]. For 1.408 eV pumping, the ratio of the signal amplitudes with helicities is unexpectedly close to the ratio of frequency shifts as would be obtained for small $\langle J_z \rangle_{\rm eq}$. This bears further investigation.

For short optical pumping times of the order of 5 s or less, a smaller shift is seen to persist after laser irradiation is turned off (Fig. 6, third set of bars). Because of the short longitudinal relaxation time of the electrons, the hyperfine-induced shift is not expected to be observed when the NMR signal is recorded in the dark; therefore the shift must have its origins in the nuclear polarization. Based on our polarization buildup data the ^{31}P polarization should be too low to create a sizable dipolar field and hence a shift in the NMR spectrum. Furthermore, the spin echo pulse sequence we employ to observe the NMR signal effectively destroys any longitudinal ^{31}P polarization; therefore the shift must be induced by ^{113,115}In. Indeed, we observe that the shift is greatly reduced if we apply a string of saturation pulses at the ^{115}In resonance frequency (Fig. 6, fourth set of bars), and that the shift remains if the indium pulses are applied off resonance (data not shown). At our field strength the Larmor frequencies of the two indium isotopes differ by only 50 kHz, so the ^{115}In pulses will have a significant effect on ^{113}In; however, the effects of ^{113}In on the ^{31}P spectrum would be expected to be small anyway given the natural abundance is only 4.3%.

There are two potential mechanisms for indium-induced ^{31}P resonance shifts (Sec. II B 2 and II B 3). We consider first the nuclear dipolar field. Large indium polarizations in our irradiated disk would create an average nuclear dipolar field at the ^{31}P sites. In the limit of 100% polarization this would induce a shift of ± 8.02 kHz. Our measured shift of 700 Hz for σ_+^B light at 1.428 eV would require a bulk indium polarization of 9% be attained with 5 s of pumping. For pumping times less than or equal to 5 s, only nuclei close to the trapped electrons will be polarized; the distance polarization can be transported by spin diffusion in 5 s is <10 nm, a reasonable estimate for the ORD Bohr radius.[33] Locally the nuclear polarization may be this large in the directly pumped sites; however, as we showed earlier, the local dipolar field from directly polarized nuclei is zero. This is borne out in our polarization buildup studies on ^{31}P, where attaining 10% polarization requires hundreds of seconds of pumping time (see Sec. IV C). This appears to rule out the average dipolar field as the source of the shift.

The second mechanism is the isotropic J coupling. The J-coupling-induced shift requires only a local population of polarized indium nuclei describable by a Zeeman spin temperature. As we showed in Sec. II B 3, our observed shift of 700 Hz can be reproduced with $J^{\rm iso} = +224$ Hz at an indium spin temperature of 11 mK, corresponding to 5% local polarization. We are not able to resolve the predicted 50 Hz narrowing of the resonance line.

This high apparent indium polarization at short pumping times is consistent with a cross-relaxation time shorter than the time for spin diffusion to equilibrate the polarization. We note, however, that the observed shift disappears at pumping times much longer than 5 s (Fig. 7). This would be expected if the indium spin diffusion is slower than that of the phosphorus, in which case the bulk of the ^{31}P signal at

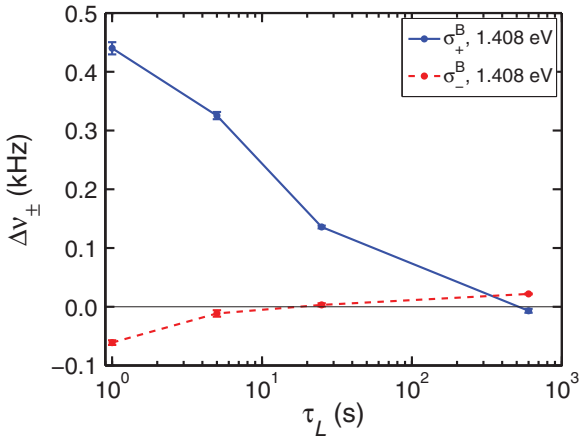

FIG. 7. (Color online) Difference between the ^{31}P NMR resonance frequencies with ^{115}In saturation *prior* to optical pumping and with ^{115}In saturation *after* optical pumping as a function of optical pumping time. In all cases, ^{31}P is saturated prior to optical pumping and data are recorded for $\tau_D = 0.1$ s.

long pumping times comes from ^{31}P with unpolarized indium neighbors. Although we would expect D for indium to be similar to that for phosphorus, if there are large electric field gradients associated with the ORD's the resulting large indium quadrupole couplings would inhibit spin diffusion.[54–56]

C. Phosphorus-induced shifts

The observation of small frequency shifts in broad lines is difficult and subject to undesirable contributions from instrumental effects. In addition, although we saturate the indium nuclei with a series of pulses after pumping has occurred, any residual indium polarization would have a disproportionate effect on the observed frequency shift, since the shift with polarization is three times higher for indium polarization than for the phosphorus polarization [Eqs. (23) and (25)]. In order to separate out these effects from measurement of the frequency shift due to the polarization of the phosphorus, the sample is subjected to a series of short radio-frequency pulses close to the phosphorus resonance frequency [Fig. 4(d), $\tau_D = 1$ s, $t_{\rm wait} = 0.1$ s], corresponding to small flip angles, and the experiment is then repeated with the opposite helicity. The shifts for the two helicities are subtracted from one another and this difference, as a function of the reduction in the phosphorus signal with number of pulses [x^N, Eq. (27)], is fit to a straight line. The slope of the line, as shown in Fig. 8, is taken as the shift with phosphorus polarization.

The data taken with 1.428 eV pumping light have a definite positive slope, which increases with pumping time, albeit at a faster rate than the NMR signal (see Table I and inset of Fig. 5). The sign of the slope is consistent with the direction of the magnetization dictated by the helicity of the light. The calculation of the average polarization from the slope of the frequency shift is given in Table I; this average is weighted by the local magnetization. Assuming an exponential decay of the nuclear polarization into the sample, and over the surface of the sample a Gaussian profile matching that of the laser beam, the maximum polarizations are given in the final column of Table I. After 1800 s of σ^B_+ 1.428 eV pumping the maximum

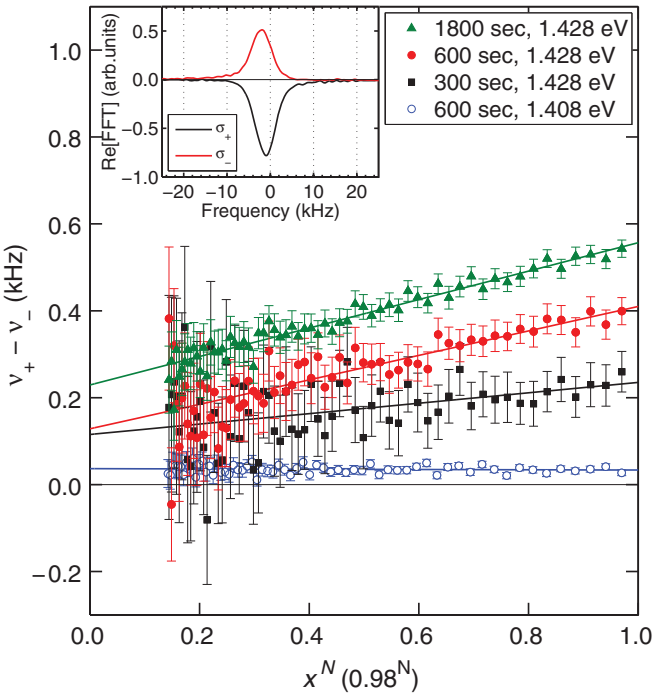

FIG. 8. (Color online) The frequency shift between helicities is given as a function of x^N, which is the reduction in signal after N θ pulses, for various pumping times at 1.428 eV (filled symbols) and for pumping at 1.408 eV (open symbols). The data are fit to a straight line, with the slope taken as the measure of the phosphorus polarization. The inset shows data acquired after the first pulse $N = 1$ and following pumping of 1800 s at 1.428 eV at the two different helicities.

polarization approaches about half the theoretical limit for the nuclear polarization of 50%.

Comparing data taken after 600 s pumping with 1.408 eV light versus 1.428 eV light reveals signal amplitudes four times larger, but frequency shifts much reduced, for the 1.408 eV data. This is consistent with the much larger penetration depth, and lower pumping efficiency, observed by Michal and Tycko for 1.408 eV versus 1.428 eV pumping.[33] Their work suggests a 16 times difference in penetration depths between pumping at the two different photon energies. In order to estimate the local ^{31}P magnetization for our data with 600 s pumping at 1.408 eV, and hence the slope of the corresponding curve in Fig. 8, we assume that the fourfold stronger signal obtained over a 16 times greater penetration depth implies a net fourfold reduction in local magnetization from that obtained at 1.428 eV. This would reduce the slope from 282 to 75 Hz/x^N. Although the size of the 1.408 eV shift is on the order of 40 Hz, the slope is not; rather the shifts appear to be rather flat with increasing number of pulses. This, however, may just show the limitations of the above technique to compensate for instrumental effects, and other potential sources of frequency shifts, for such a several kilohertz broad peak.

We can also calculate the polarization from the ratio of the optically pumped signal $S_{\pm}$ to the thermal equilibrium signal from the entire sample $S_{\rm eq}$ after saturation of both indium and phosphorus lines and recovery in the dark for time $t_{\rm wait}$. This

TABLE I. For increasing pump times at 1.428 eV (first column) the amplitude of the initial signal in the pulse train is given for both positive S_+ and negative S_- helicities, along with the frequency shift between the helicities as a function of signal reduction with repeated pulses. From the amplitudes and this frequency shift, the average polarizations $\langle P_+\rangle$ and $\langle P_-\rangle$ are calculated, as well as the maximum polarization at the surface of the sample. The latter assumes an exponential decay of the polarization into the sample from the surface and a Gaussian surface profile matching the laser beam profile.

1.428 eV pump time (s)	S_+	S_-	Shift slope (Hz/x^N)	$\langle P_+\rangle$%	$\langle P_-\rangle$%	$P_{\max^+}$%	$P_{\max^-}$%
300	0.394 ± 0.003	0.230 ± 0.002	120 ± 44	3.1 ± 1.1	1.8 ± 0.7	9 ± 3	5 ± 2
600	0.620 ± 0.002	0.391 ± 0.002	282 ± 29	7.0 ± 0.7	4.4 ± 0.5	20 ± 2	13 ± 1
1800	1.000 ± 0.002	0.653 ± 0.002	328 ± 17	8.1 ± 0.4	5.3 ± 0.3	23 ± 1	15 ± 1

ratio can be expressed as

$$\frac{S_\pm}{S_{\rm eq}} = \frac{P_{\max}}{P_{\rm eq}\left(1 - e^{-\frac{t_{\rm wait}}{T_1}}\right)} \times \frac{\iiint e^{-2\frac{(x^2+y^2)}{w^2}} e^{-\frac{z}{d}} dxdydz}{\iiint dxdydz}, \quad (28)$$

where $P_{\max}$ is the maximum surface polarization from optical pumping, $P_{\rm eq}$ is the thermal equilibrium polarization, d is the penetration depth, $w = 3.7$ mm characterizes the spot size of the laser, T_1 is the spin-lattice relaxation time, and the integration is over the dimensions of the sample ($8 \times 4.5 \times 0.35$ mm). We define the second fraction on the right-hand side of Eq. (28) as R, the fraction of the volume which is optically pumped. Using the penetration depths measured by Michal and Tycko,[33] we calculate for our two photon energies the fractional volumes $R_{1.428} \approx 0.003$ and $R_{1.408} \approx 0.06$.

Using a different sample fragment than that used to obtain the data in Table I, polarizations were obtained for both light helicities from signals after 600 s of pumping as well as a thermal equilibrium signal. The optically pumped data and thermal polarization data were taken back-to-back to ensure uniform experimental conditions; representative data are shown in Fig. 1. For 600 s of 1.408 eV pumping, we obtain maximum polarizations of 4 ± 1% and 2.0 ± 0.5% for σ_+^B and σ_-^B light, respectively. For 600 s of pumping at 1.428 eV, we obtain 7 ± 2% and 6 ± 2% maximum polarization for σ_+^B and σ_-^B light, respectively. Using the frequency shift of 70 ± 31 Hz/x^N for the same set of data we find $\langle P_+\rangle = 1.6 \pm 0.7$% and $\langle P_-\rangle = 1.3 \pm 0.6$%, or a maximum polarization of $P_{\max^+} = 5 \pm 2$% and $P_{\max^-} = 4 \pm 2$%, again assuming an exponential decay into the sample and a Gaussian profile matching that of the laser beam. One would expect the maximum polarization calculated by both techniques to be similar, and indeed they are in good agreement. For the same pumping times, these polarization values and those from Table I from another sample are different. We are not certain of the reason for the difference in polarization level between the two samples, but speculate that it may be caused by slight differences in surface treatment and history.

V. CONCLUSIONS

We have observed resonance shifts in the ^{31}P NMR spectra of optically pumped InP. During pumping, particularly for short pumping times, the dominant shift mechanism is hyperfine coupling to the spin-polarized electrons. After the light is turned off, smaller shifts persist. These shifts are due to the dipolar fields of, and J couplings to, the highly polarized nuclei, and can be used as a quantitative measure of the nuclear polarization. We expect that this approach will be applicable to other optically pumped semiconductors.

The shift due to spin-polarized indium dominates the ^{31}P spectrum through the J coupling "in the dark" at short pumping times. The indium polarization value calculated from the shift induced by 5 s of pumping is 5% at 1.428 eV. At pumping times longer than a few tens of seconds the indium-induced shift disappears. We hypothesize that the indium polarization does not spread as rapidly by spin diffusion as does the phosphorus polarization, leading to the bulk of the ^{31}P signal coming from phosphorus surrounded by unpolarized indium at long pumping times.

Shifts in the ^{31}P spectrum attributable to ^{31}P dipolar fields are also observed at long pumping times for our InP system. The average polarization calculated from these shift data is in agreement with the polarization calculated from signal size and volume of the pumped region. As expected, we observe an increase of polarization with pumping time and, using the shift data, we calculate polarizations as high as 23% for the longest pumping time. This polarization is comparable to that obtained with the same material at much higher fields and much longer pumping times.[33]

Our results have significance for attempts to develop an optical nuclear spin polarizer using the ^{31}P nuclei in optically pumped InP as a source.[4] They show going to lower magnetic fields (2.35 T) than previously used with circularly polarized irradiation favorably increases the polarization rate, and that very substantial polarizations can be achieved despite the reduction in the T_1 of the ^{31}P nuclei at lower field. We also observe, as did Michal and Tycko at higher field,[33] that although below-gap irradiation at 1.408 eV produces the larger ^{31}P total signal, above-gap irradiation at 1.428 eV produces a higher polarization density in a smaller region closer to the surface, and thus is more desirable for polarization-transfer approaches. Experiments are now commencing to assess the degree of nuclear polarization at the very surface (interface) of InP, and to transfer the polarization to surface-bound species.

ACKNOWLEDGMENTS

We wish to thank Dr. Robert Tycko for providing the Fe-doped InP sample used in these studies, Dr. Sean Hart for the use of his lasers, and Professor Jerry Miller for help with probe construction. This work was supported by the Office of Naval Research. One of us (KLS) acknowledges support in part by NSF Grant No. 0547987.

*Author to whom correspondence should be addressed.
[1]G. Lampel, Phys. Rev. Lett. **20**, 491 (1968).
[2]S. E. Hayes, S. Mui, and K. Ramaswamy, J. Chem. Phys. **128**, 052203 (2008).
[3]J. A. Reimer, Solid State Nucl. Magn. Reson. **37**, 3 (2010).
[4]R. Tycko, Solid State Nucl. Magn. Reson. **11**, 1 (1998).
[5]L. Goehring and C. A. Michal, J. Chem. Phys. **119**, 10325 (2003).
[6]A. Goto, T. Shimizu, K. Hashi, S. Ohki, T. Iijima, and G. Kido, IEEE Trans. Appl. Supercond. **14**, 1635 (2004).
[7]J. Schliemann, A. Khaetskii, and D. Loss, J. Phys. Condens. Matter **15**, R1809 (2003).
[8]I. Zutic, J. Fabian, and S. DasSarma, Rev. Mod. Phys. **76**, 323 (2004).
[9]A. Goto, T. Shimizu, K. Hashi, H. Kitazawa, and S. Ohki, Phys. Rev. A **67**, 022312 (2003).
[10]B. E. Kane, Nature (London) **393**, 133 (1998).
[11]W. A. Coish and J. Baugh, Phys. Status Solidi B **246**, 2203 (2009).
[12]A. K. Paravastu and J. A. Reimer, Phys. Rev. B **71**, 045215 (2005).
[13]S. K. Buratto, D. N. Shykind, and D. P. Weitekamp, Phys. Rev. B **44**, 9035 (1991).
[14]K. Ramaswamy, S. Mui, and S. E. Hayes, Phys. Rev. B **74**, 153201 (2006).
[15]K. Ramaswamy, S. Mui, and S. E. Hayes, Phys. Rev. B **75**, 249903(E) (2007).
[16]P. J. Coles, Phys. Rev. B **78**, 033201 (2008).
[17]P. J. Coles and J. A. Reimer, Phys. Rev. B **76**, 174440 (2007).
[18]G. Fisher and C. Hermann, Phys. Status Solidi B **63**, 307 (1974).
[19]P. Y. Yu and M. Cardona, *Fundamentals of Semiconductors: Physics and Materials Properties*, 4th ed. (Springer, Berlin, 2010).
[20]C. Weisbuch and C. Hermann, Phys. Rev. B **15**, 816 (1977).
[21]W. Farah, M. Dyakonov, D. Scalbert, and W. Knap, Phys. Rev. B **57**, 4713 (1998).
[22]C. Weisbuch and C. Hermann, Solid State Commun. **16**, 659 (1975).
[23]B. Gotschy, G. Denninger, H. Obloh, W. Wilkening, and J. Schneider, Solid State Commun. **71**, 629 (1989).
[24]B. Clerjaud, F. Gendron, H. Obloh, J. Schneider, and W. Wilkening, Phys. Rev. B **40**, 2042 (1989).
[25]P. Lawaetz, Phys. Rev. B **4**, 3460 (1971).
[26]D. Paget, Phys. Rev. B **25**, 4444 (1982).
[27]A. Patel, O. Pasquet, J. Bharatam, E. Hughes, and C. R. Bowers, Phys. Rev. B **60**, 5105 (1999).
[28]J. D. Jackson, *Classical Electrodynamics*, 3rd ed. (Wiley, Hoboken, NJ, 1988).
[29]D. Paget, G. Lampel, B. Sapoval, and V. I. Safarov, Phys. Rev. B **15**, 5780 (1977).
[30]C. P. Slichter, *Principles of Magnetic Resonance*, Series in Solid-State Sciences, 3rd ed. (Springer, Heidelberg, 1996).
[31]P. L. Kuhns, A. Kleinhammes, T. Schmiedel, W. G. Moulton, E. Hughes, S. Sloan, P. Chabrier, and C. R. Bowers, Phys. Rev. B **55**, 7824 (1997).
[32]A. Abragam, *The Principles of Nuclear Magnetism* (Clarendon, Oxford, 1961).
[33]C. A. Michal and R. Tycko, Phys. Rev. B **60**, 8672 (1999).
[34]A. Goto, K. Hashi, T. Shimizu, R. Miyabe, X. Wen, S. Ohki, S. Machida, T. Iijima, and G. Kido, Phys. Rev. B **69**, 075215 (2004).
[35]E. Burstein, G. S. Picus, R. F. Wallis, and F. Blatt, Phys. Rev. **113**, 15 (1959).
[36]S. Mui, K. Ramaswamy, C. J. Stanton, S. A. Crooker, and S. E. Hayes, Phys. Chem. Chem. Phys. **11**, 7031 (2009).
[37]K. Ramaswamy, S. Mui, S. A. Crooker, X. Pan, G. D. Sanders, C. J. Stanton, and S. E. Hayes, Phys. Rev. B **82**, 085209 (2010).
[38]P. Rochon and E. Fortin, Phys. Rev. B **12**, 5803 (1975).
[39]L. Pavesi, F. Piazza, A. Rudra, J. F. Carlin, and M. Ilegems, Phys. Rev. B **44**, 9052 (1991).
[40]M. Engelsberg and R. E. Norberg, Phys. Rev. B **5**, 3395 (1972).
[41]O. H. Han, H. K. C. Timken, and E. Oldfield, J. Chem. Phys. **89**, 6046 (1988).
[42]N. L. Adolphi, M. S. Conradi, and W. E. Buhro, J. Phys. Chem. Solids **53**, 1073 (1992).
[43]M. Tomaselli, D. deGraw, J. L. Yarger, M. P. Augustine, and A. Pines, Phys. Rev. B **58**, 8627 (1998).
[44]T. Iijima, K. Hashi, A. Goto, T. Shimizu, and S. Ohki, Chem. Phys. Lett. **419**, 28 (2006).
[45]D. Paget and V. L. Berkovits, in *Optical Orientation*, edited by F. Meier and B. P. Zakharchenya (North-Holland, Amsterdam, 1984).
[46]A. Brunetti, M. Vladimirova, D. Scalbert, H. Folliot, and A. Lecorre, Phys. Rev. B **73**, 121202 (2006).
[47]G. Deville, M. Bernier, and J. M. Delrieux, Phys. Rev. B **19**, 5666 (1979).
[48]P. Hodgkinson, D. Sakellariou, and L. Emsley, Chem. Phys. Lett. **326**, 515 (2000).
[49]J. Jeener, Phys. Rev. Lett. **82**, 1772 (1999).
[50]K. L. Sauer, F. Marion, P. J. Nacher, and G. Tastevin, Phys. Rev. B **63**, 184427 (2001).
[51]D. J. Griffiths, *Introduction to Electrodynamics*, 3rd ed. (Prentice Hall, Upper Saddle River, NJ, 1999).
[52]S. Mui, K. Ramaswamy, and S. E. Hayes, Phys. Rev. B **75**, 195207 (2007).
[53]C. A. Michal and R. Tycko, Phys. Rev. Lett. **81**, 3988 (1998).
[54]I. J. Lowe and D. Tse, Phys. Rev. **166**, 279 (1968).
[55]A. G. Redfield and W. N. Yu, Phys. Rev. **169**, 443 (1968).
[56]A. G. Redfield and W. N. Yu, Phys. Rev. **177**, 1018 (1969).